

# UrbanCross: Enhancing Satellite Image-Text Retrieval with Cross-Domain Adaptation

Siru Zhong<sup>1</sup>, Xixuan Hao<sup>1</sup>, Yibo Yan<sup>1</sup>, Ying Zhang<sup>2</sup>, Yangqiu Song<sup>3</sup>, Yuxuan Liang<sup>1†</sup>

<sup>1</sup>The Hong Kong University of Science and Technology (Guangzhou), <sup>2</sup>Northwestern Polytechnical University

<sup>3</sup>The Hong Kong University of Science and Technology

{szhong691,xhao390}@connect.hkust-gz.edu.cn;yanyibo70@gmail.com  
izhangying@nwpu.edu.cn;yqsong@cse.ust.hk;yuxliang@outlook.com

## ABSTRACT

Urbanization challenges underscore the necessity for effective satellite image-text retrieval methods to swiftly access specific information enriched with geographic semantics for urban applications. However, existing methods often overlook significant domain gaps across diverse urban landscapes, primarily focusing on enhancing retrieval performance within single domains. To tackle this issue, we present UrbanCross, a new framework for cross-domain satellite image-text retrieval. UrbanCross leverages a high-quality, cross-domain dataset enriched with extensive geo-tags from three countries to highlight domain diversity. It employs the Large Multimodal Model (LMM) for textual refinement and the Segment Anything Model (SAM) for visual augmentation, achieving a fine-grained alignment of images, segments and texts, yielding a 10% improvement in retrieval performance. Additionally, UrbanCross incorporates an adaptive curriculum-based source sampler and a weighted adversarial cross-domain fine-tuning module, progressively enhancing adaptability across various domains. Extensive experiments confirm UrbanCross’s superior efficiency in retrieval and adaptation to new urban environments, demonstrating an average performance increase of 15% over its version without domain adaptation mechanisms, effectively bridging the domain gap.

## CCS CONCEPTS

• **Information systems** → **Specialized information retrieval**.

## KEYWORDS

Satellite image-text retrieval; Cross-domain adaptation; Multimodal

## 1 INTRODUCTION

Enriched with geographic details, satellite imagery serves as a vital resource for comprehending the functionality of a region, with a variety of applications ranging from poverty assessment [18, 19], crop yield prediction [34, 35], to urban region profiling [13, 44]. *Satellite Image-Text Retrieval* aims to retrieve specific satellite images from an image pool based on text descriptions, and vice versa [3], which has gathered increased attention with global urbanization. The key to the success of such retrieval lies in effectively harmonizing satellite image and textual data within urban complexities [53].

Related literature can be categorized into two main paradigms [20, 22, 52]. The first stream, known as *Content-based methods*, is centered on generating precise captions for satellite images via generative models, converting image-text retrieval to a text-to-text task [23, 42]. However, these methods usually encounter detail loss in complex scenes and heavily rely on extensive annotated datasets.

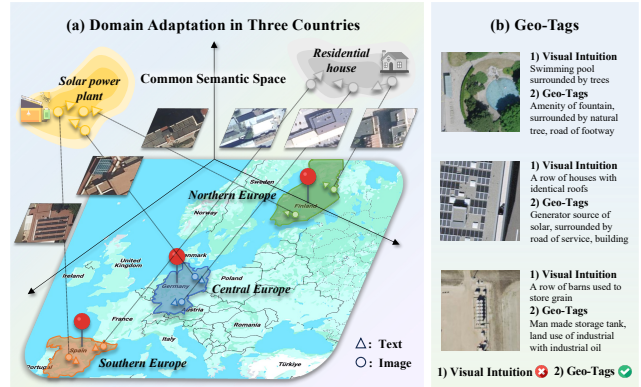


**Figure 1: (a) Domain adaptation for differentiating solar power plants from residential houses across countries. (b) Geo-tags can complement visual intuition.**

In contrast, *Embedding-based methods* aim to leverage pre-trained encoders to align images and texts within a unified semantic space, ensuring better modal interaction for the retrieval task. These approaches explore novel mechanisms, such as self-attention and Contrastive Language-Image Pre-training (CLIP), to enhance representation learning [24, 33, 39] and modality interaction [9, 46].

Though promising, previous approaches mostly assume uniformity in satellite image-text pairs across varied landscapes. This assumption, however, may lead to inferior model performance when dealing with data distribution shifts. Figure 1(a) depicts an example, where geographical differences, such as the varying prevalence of solar power plants between Finland and Spain due to distinct solar exposure levels, may result in the model trained on Finnish data incorrectly classifying Spanish solar plants as residential areas. This underscores the critical need for cross-domain adaptation to ensure semantically equivalent feature alignment across geographies.

In this paper, we identify two key perspectives to enhance satellite image-text retrieval with cross-domain adaptation

- *Data perspective*: Learning domain-invariant features is the prerequisite for cross-domain adaptation. When understanding urban regions, relying solely on visual features may lead to misinterpretation, as illustrated in Figure 1(b). Fortunately, real-world satellite images are often accompanied by other descriptions or metadata, such as geo-tags, which are texts that can generalize well in all countries. By incorporating such auxiliary information, we can effectively identify and complement

original vision representations, thereby enhancing the generalization ability of retrieval models.

- **Model perspective:** Enhancing the model’s adaptability to domain shifts requires improving the identification and adjustment capabilities to data variances across domains, through a robust and domain-aware framework. Our approach dynamically adjusts model parameters in response to identified domain-specific features, thereby significantly improving the adaptability and accuracy of the retrieval system.

In response to these challenges, we present a novel framework termed **UrbanCross**, which enhances the embedding-based retrieval paradigm with *cross-domain adaptability*. From the data perspective, we augment data representations with two endeavors. Externally, our model integrates geo-tags with Large Multimodal Model (LMM) to generate visually rich and semantically accurate image captions. Internally, we employ Segment Anything (SAM) to extract fine-grained visual features from the input image itself, eliminating irrelevant elements and aligning these with corresponding text to enhance data quality across visual and language domains.

From the model perspective, we devise two innovative modules: *Adaptive Curriculum-based Source Sampler*, which initially samples source data based on similarity to the target domain, followed by the *Adversarial Cross-Domain Image-Text Fine-tuning Module* for subsequent fine-tuning. This integrated strategy ensures a seamless transition from simpler to complex samples, applying weighting to align with domain-specific traits, thus effectively addressing the challenges posed by diverse data distributions across domains.

Our contributions are summarized as follows:

- **Data Augmentation:** By integrating LMM with geo-tags to enrich textual descriptions and employing SAM for precise visual segmentation, UrbanCross significantly enhances both visual and textual accuracy, ensuring contextual and semantic understanding, resulting in higher-quality data representations.
- **Cross-Domain Adaptation:** We introduce a curriculum-based source sampler and a weighted adversarial fine-tuning module. This integration significantly improves domain adaptation by enhancing the accuracy of multimodal fusion across images, texts, and segmented visual elements.
- **Extensive experiments:** Through extensive comparative and cross-country testing, UrbanCross has achieved a 10% improvement in retrieval performance and a 15% average boost over methods lacking domain adaptation.

## 2 PRELIMINARIES

### 2.1 Formulation

**Definition 1 (Satellite Image):** A satellite image  $I_g$  representing an urban area  $g$  can be denoted as in  $\mathbb{R}^{H \times W \times 3}$ , where  $H$  and  $W$  are length and width. It includes Ground Sample Distance (GSD) for spatial resolution, geographical coordinates for precise positioning, and geo-tags providing contextual information like location-based labels to aid in object recognition within urban environments.

**Definition 2 (Image Captioning):** The textual description  $T_g$  of a satellite image  $I_g$  is generated by LMM, producing captions that integrate visual content and geo-tags. This enriches the understanding of urban features and aids in identifying key objects.

**Problem Statement (Cross-Domain Satellite Image-Text Retrieval):** Given dataset  $D_s = \{(I_{g_i}, T_{g_i})\}_{i=1}^{N_s}$  from a source domain, and  $D_t = \{(I_{g'_i}, T_{g'_i})\}_{i=1}^{N_t}$  from a target domain, where  $N_s$  and  $N_t$  represent the respective lengths of the datasets. The goal is to develop a model  $\mathcal{F}$  that maps image-text pairs to vectors within an embedding space that aligns and generalizes across domains. Consequently, the representation vectors  $\mathbf{e}_g^I, \mathbf{e}_g^T = \mathcal{F}(I_g, T_g)$  can facilitate efficient image-to-text (i2t) and text-to-image (t2i) retrieval tasks.

### 2.2 Related Work

**2.2.1 Satellite Image-Text Retrieval.** Recent developments in satellite image-text retrieval have improved alignment between textual and visual data. Enhanced by neural network architectures like CNNs, RNNs, and Transformers, these advancements foster robust feature extraction and modality interactions [8, 14, 28, 36, 46, 48, 49]. Techniques such as GaLR [49] and KCR [28] have advanced text comprehension by integrating global-local image features and domain-specific knowledge, respectively. Meanwhile, Vision-Language Pre-training (VLP) models like CLIP [33] face challenges in processing diverse urban satellite imagery features. Innovations in high-resolution imaging [39] and multilingual text processing [2] highlight VLP’s adaptability, supported by foundational models such as RSGPT [16] and SkyEyeGPT [50]. However, these methods often neglect the data distribution variability across different domains, an issue UrbanCross aims to address.

**2.2.2 Large Multimodal Model and Segment Anything Model.** With the rapid advancements in Large Language Model (LLM), the incorporation of visual information into these models is increasingly prominent. Recent developments, including MiniGPT-4 [4], LLaVA [26], and InstructBLIP [10], have expanded parameters and training data, contributing to the evolution of LMM. Models such as mPLUG-Owl [45], Shikra [6], and KOSMOS-2 [32] have introduced techniques aimed at mitigating hallucinations in LMM. Concurrently, SAM [21], renowned for its robust image segmentation capabilities, finds widespread application across various domains. This includes urban infrastructure analysis [1], UV-SAM for urban segmentation [51], and RSPrompter for satellite image-based instance segmentation [5]. Yet, the potential of these models in satellite image-text retrieval remains largely untapped. Hence, UrbanCross leverages the strengths of LMM and SAM to enrich the image-text dataset, facilitating multimodal alignment and cross-domain adaptation.

**2.2.3 Domain adaptation in Urban Research.** Domain adaptation, a critical subfield of transfer learning, is pivotal in overcoming labeled data scarcity and ensuring model generalization across varied scenarios [31]. In urban areas, the application of domain adaptation is invaluable, leveraging heterogeneous data to markedly enhance model performance in areas such as traffic forecasting [37], environmental monitoring [41], and air quality prediction [40]. Despite its widespread application in urban contexts, domain adaptation strategies remain underexplored in satellite image-text retrieval. UrbanCross addresses this gap by incorporating domain adaptation strategies for satellite imagery and its associated texts, thus enhancing adaptability across global urban landscapes.

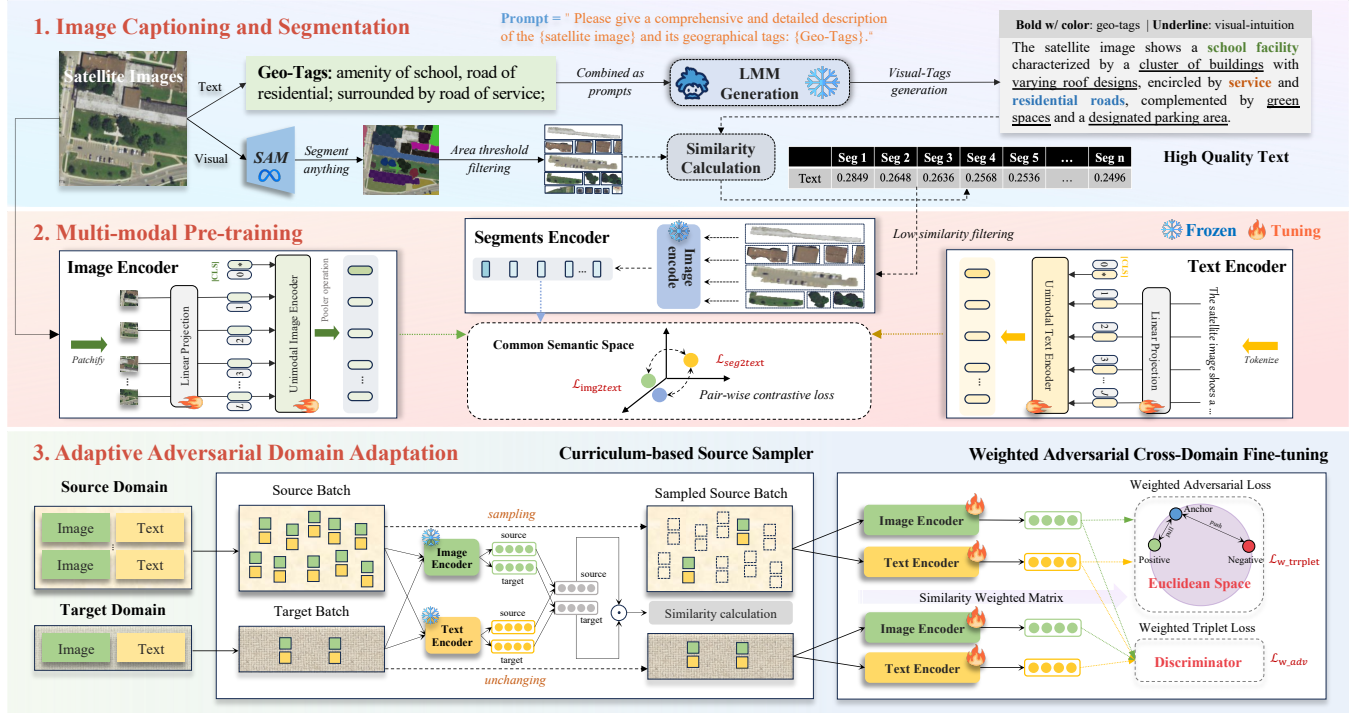


Figure 2: Overall framework of the proposed UrbanCross.

### 3 METHODOLOGY

The UrbanCross framework (Figure 2) has three main stages.

- **Image Captioning and Segmentation:** At stage one, LMM, augmented with geo-tags, produces detailed descriptions for satellite images, yielding semantically enriched image-text pairs. Simultaneously, SAM [21] is utilized to segment the image, removing irrelevant areas through area assessment and text similarity comparison, ensuring fine-grained feature extraction for fusion.
- **Multi-Modal Pre-training:** At stage two, images, segments, and texts are encoded independently, then merged into a unified semantic space using pairwise contrastive loss to bring similar ones closer together while pushing dissimilar ones farther apart.
- **Adaptive Adversarial Domain Adaptation:** At stage three, batches from source and target domains are processed by an adaptive curriculum-based sampler. Using the pre-trained encoder, it first transforms image-text pairs into representations, then evaluates domain similarity and progressively excludes source batches, starting with those most similar to the target (easy) to those least similar (hard). Subsequently, refined batches and target domain data undergo adversarial cross-domain fine-tuning, minimizing weighted contrastive and discriminator losses. Unimodal encoders are then fine-tuned for domain alignment.

#### 3.1 Image Captioning and Segmentation

**3.1.1 Text Augmentation with LMM and Geo-Tags.** To ensure high-quality textual descriptions for experiments, we employ the Instruct-CLIP [10] LLM for text generation. However, directly inputting satellite images into the LLM can result in insufficient semantic details. As illustrated in phase 1 of Figure 2, although the model

captures general features like "cluster of buildings", "parking areas", and "green spaces", it often omits specific details such as "residential roads" or "school facilities". To address this, geo-tags are integrated to enhance visual accuracy and provide additional contextual information, resulting in n more detailed and precise image captions.

**3.1.2 Image Augmentation with SAM.** In satellite image-text retrieval tasks, precisely matching text details with image features is crucial. However, extraneous elements in satellite images often reduce accuracy. We address this using SAM [21], to isolate key features from images. We initially set an area threshold in SAM's "everything" mode to exclude overly small and non-essential segments, for further improving visual-language alignment.

$$\mathbf{S}_{filtered} = \{\mathbf{s}_i | area(\mathbf{s}_i) > \mathbf{T}_a, \mathbf{s}_i \in \mathbf{S}\}, \quad (1)$$

Here,  $\mathbf{S}_{filtered}$ , derived by applying an area threshold  $\mathbf{T}_a$  to the original segment collection  $\mathbf{S}$ , excludes smaller segments. CLIP [33] is then used to calculate the similarity between text and segments.

$$score(\mathbf{s}_i, \mathbf{t}) = \langle \phi_{seg}(\mathbf{s}_i), \psi_{text}(\mathbf{t}) \rangle, \quad (2)$$

$$\mathbf{S}_{semantic} = \{\mathbf{s}_i | score(\mathbf{s}_i, \mathbf{t}) > \mathbf{T}_s, \mathbf{s}_i \in \mathbf{S}_{filtered}\}, \quad (3)$$

where  $score(\mathbf{s}_i, \mathbf{t})$  measures segment-text similarity, and  $\phi_{seg}$  and  $\psi_{text}$  are the respective CLIP encoders, segments meeting this criterion are weighted in the final embedding.

$$\mathbf{E}_{\mathbf{S}} = \frac{\sum_{i=1}^n \mathbf{w}_i \cdot \phi_{seg}(\mathbf{s}_i)}{\sum_{i=1}^n \mathbf{w}_i}, \quad (4)$$

where  $\mathbf{w}_i = score(\mathbf{s}_i, \mathbf{t})$  serves as the weight for each segment, prioritizing the most relevant ones, ensuring a focused and semantically coherent alignment with textual descriptions.

## 3.2 Multi-modal Pre-training

**3.2.1 Learning Satellite Image Representations.** Satellite image representations are learned using the CLIP Vision Transformer (ViT-L-14). The image  $I_g$  is segmented into  $16 \times 16$  pixel patches  $I_p$ , projected to  $E_p^I = \mathbf{W}_p^I p^\top + b_p$  with positional embeddings  $E_{pos}$  added to enhance spatial information. The resulting embeddings  $E_e^I = E_p^I + E_{pos}$  undergo self-attention processing, including multi-head mechanisms (MSA).

$$(\mathbf{Q}^I, \mathbf{K}^I, \mathbf{V}^I)^\top = E_e^I (\mathbf{W}_Q, \mathbf{W}_K, \mathbf{W}_V)^\top, \quad (5)$$

$$E_{(i)}^I = \text{Softmax}\left(\frac{\mathbf{Q}^I \mathbf{K}^{I\top}}{\sqrt{d}}\right) \mathbf{V}^I, \quad (6)$$

$$E_{MSA}^I = \text{Concat}(E_{(1)}^I, E_{(2)}^I, \dots, E_{(N_h)}^I) \mathbf{W}_O, \quad (7)$$

where  $\mathbf{W}_O$  is the learnable output projection matrix,  $N_h$  is the number of heads, and  $\text{Concat}$  indicates concatenation operation. Self-attention dynamically weights the interactions between patches, enhanced by residual connections and layer normalization, producing the latent visual representation:

$$E^I = \text{LayerNorm}(E_e^I + E_{MSA}^I). \quad (8)$$

Building on the dynamic patch representations achieved through self-attention and layer normalization, this approach also incorporates a learnable image [CLS] token to further enhance visual encodings for complex cross-modality tasks.

**3.2.2 Learning Text Representations.** Text descriptions for satellite images, enhanced by LMM and geo-tags, are processed using a Transformer-Encoder [38]. The text encoder follows a similar MSA mechanism of the visual encoder. The input text sequence is bracketed with [SOS] and [EOS] tokens, and the activation of the highest layer of Transformer at [EOS] token is considered the global representation  $E^T$  of text.

**3.2.3 Pair-wise Modal Alignment.** To achieve finer feature alignment between visual and language modalities, we enhance retrieval accuracy by creating a shared embedding space that bridges the semantic gap between satellite images (EI), image segments (ES), and text (ET). This uses pairwise contrastive loss to align images and segments with text, assessing their similarities, respectively:

- **Image-to-Text Contrastive Loss ( $\mathcal{L}_{img2text}$ ):** Reduces disparities between matched image-text pairs while enhancing the distinction for mismatches.
- **Segment-to-Text Contrastive Loss ( $\mathcal{L}_{seg2text}$ ):** Improves the alignment between image segments and corresponding text, promoting proximity for related pairs while increasing separation for unrelated ones.

The total objective function,  $\mathcal{L} = \mathcal{L}_{img2text} + \mathcal{L}_{seg2text}$ , guides the model in tightly aligning images and segments with textual descriptions. By employing margin-driven separation in the embedding space, this contrastive approach enhances the model's ability to differentiate between related and unrelated pairs.

## 3.3 Adaptive Adversarial Domain Adaptation

**3.3.1 Adaptive Curriculum-based Source Sampler.** The disparity in data distribution between source and target domains hampers domain adaptation. To address this, we introduce the Adaptive

Curriculum-based Source Sampler (ACSS), which progressively integrates more challenging source samples (characterized by their complexity and relevance to the challenges in the target domain) during training. This strategy ensures smooth adaptation to data distribution changes and maintains performance when fine-tuned with limited data. Initially, we concurrently iterate through the source and target datasets with varying data volumes, i.e., batch sizes, selecting a target batch of  $n^t$  pairs and a source batch consisting of  $n^s = 5 * n^t$  image-text pairs. Features are extracted from these image-text pairs using frozen pre-trained encoders. These are denoted by  $E_p^s = \{E_{p_i}^s\}_{i=1}^{n^s}$  and  $E_p^t = \{E_{p_i}^t\}_{i=1}^{n^t}$ , where  $E_{p_i}^s$  and  $E_{p_i}^t$  signify the aggregated features of text and images. A similarity matrix  $\mathbf{W}_1 \in \mathbb{R}^{n^t \times n^s}$  is then computed to assess the pairwise similarities between the target and source batches, quantifying the degree of alignment between features.

$$\mathbf{W}_1(j, i) = \frac{E_{p_j}^t \cdot E_{p_i}^s}{\|E_{p_j}^t\| \|E_{p_i}^s\|}. \quad (9)$$

Based on  $\mathbf{W}_1$ , we extract a new source subset by selecting the top  $K\%$  most similar pairs for each target. The curriculum learning strategy incrementally increases  $K$  from 0 by 20% across five epochs, progressing from simpler to more complex samples. Specifically, the range initially covers the first 20%, and then expanding in subsequent epochs to include the next 20% increments, i.e., from 20% to 40%, then from 40% to 60%, and so on. This method ensures progressive exposure from simpler to more complex samples, enhancing adaptation without introducing additional overhead.

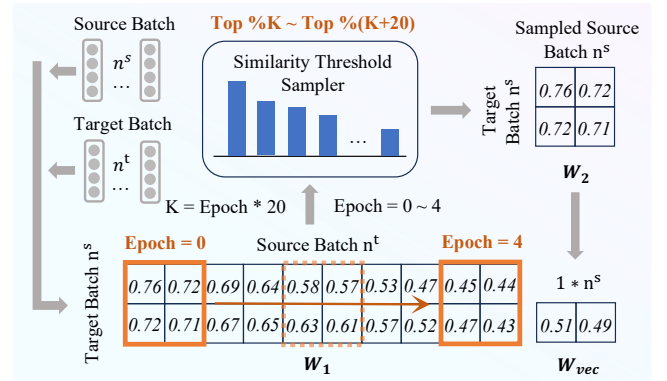


**Figure 3: The similarity matrix between source/target image-text pairs gradually transforms into the weight vector.**

Additionally,  $\mathbf{W}_2 \in \mathbb{R}^{n^t \times n}$ , derived from  $\mathbf{W}_1$ , reflects evolving similarity between selected source and target batches. Continuously updated, these matrices guide the choice of increasingly challenging source batches. Consequently, the ACSS-selected matrix supports weighted adversarial learning, enhancing domain adaptation.

**3.3.2 Weighted Adversarial Cross-Domain Fine-tuning.** Weighted cross-modal adversarial learning enhances performance by selectively emphasizing source samples similar to target data and reducing the impact of dissimilar ones. As depicted in Figure 2, shared visual and textual encoders process features from both source and target image-text pairs, denoted as  $\tilde{\mathbf{E}}_T^s = \{(\tilde{\mathbf{E}}_{T_i^s}^s)\}_{i=1}^n$ ,  $\tilde{\mathbf{E}}_I^s = \{(\tilde{\mathbf{E}}_{I_i^s}^s)\}_{i=1}^n$ ,

$\tilde{\mathbf{E}}_T^t = \{(\tilde{\mathbf{E}}_{T_j^t})\}_{j=1}^n$  and  $\tilde{\mathbf{E}}_I^t = \{(\tilde{\mathbf{E}}_{I_j^t})\}_{j=1}^n$  for batch size  $n$ . Based on ACSS-selected matrix  $W_2$ , we get a weight vector  $\mathbf{W}_{vec}$  through sum up and normalize across the target dimension, assigns weights to each source sample in training, where  $\mathbf{S}$  represents vector elements equal to the sum of each row, specifically,  $\mathbf{S}(i) = \sum_{j=1}^n \mathbf{W}_2(i, j)$ .

$$\begin{aligned} \mathbf{W}_{vec}(i) &\leftarrow \frac{\mathbf{S}(i) - \min(\mathbf{S})}{\max(\mathbf{S}) - \min(\mathbf{S})} \\ \mathbf{W}_{vec}(i) &\leftarrow \frac{n \cdot \mathbf{W}_{vec}(i)}{\sum_{i=1}^n \mathbf{W}_{vec}(i)} \end{aligned} \quad (10)$$

The training employs an objective function  $\mathcal{L} = \mathcal{L}_{w\_triplet}^s + \beta \mathcal{L}_{w\_adv}$ , where  $\beta$  modulates the balance between weighted triplet and adversarial losses, with the superscript  $s$  indicating that these losses are specific to the source domain. The weighted triplet loss aims to bring positive pairs closer and separate negative pairs, adjusting source data weights during its computation to bridge the gap between source and target domains:

$$\begin{aligned} \mathcal{L}_{w\_triplet}^s &= \mathbf{W}_{vec} [d(\tilde{\mathbf{E}}_{T_a^s}, \tilde{\mathbf{E}}_{I_p^s}) - d(\tilde{\mathbf{E}}_{T_a^s}, \tilde{\mathbf{E}}_{I_n^s}) + \alpha]_+ \\ &+ \mathbf{W}_{vec} [d(\tilde{\mathbf{E}}_{I_a^s}, \tilde{\mathbf{E}}_{T_p^s}) - d(\tilde{\mathbf{E}}_{I_a^s}, \tilde{\mathbf{E}}_{T_n^s}) + \alpha]_+, \end{aligned} \quad (11)$$

Here,  $d(\cdot, \cdot)$  denotes the cosine similarity distance, with  $a$ ,  $p$ , and  $n$  representing anchor, positive, and negative samples, respectively. The term  $\alpha$  refers to the margin. A domain discriminator  $D$ , implemented by a three-layer MLP, is utilized to align source and target domain distributions. During training,  $D$  minimizes binary cross-entropy loss between its predictions and ground truth labels, indicating real or generated data. With source  $(\tilde{\mathbf{E}}_T^s, \tilde{\mathbf{E}}_I^s)$  and target  $(\tilde{\mathbf{E}}_T^t, \tilde{\mathbf{E}}_I^t)$  features as input,  $D$  is adversarially trained with the encoder to predict domain labels. The encoders for text and images are fine-tuned to produce image-text features indistinguishable by  $D$ , which seeks to maximize the probability of correct predictions.

$$\mathcal{L}_{w\_adv} = \mathbf{W}_{vec} \log D(\tilde{\mathbf{E}}_T^s, \tilde{\mathbf{E}}_I^s) + \mathbf{W}_{vec} \log(1 - D(\tilde{\mathbf{E}}_T^t, \tilde{\mathbf{E}}_I^t)). \quad (12)$$

## 4 EXPERIMENTS

In this section, we conduct extensive experiments to investigate the following Research Questions (RQ):

- **RQ1:** Can UrbanCross outperform previous methods without domain adaptation? How does the inclusion of segmented images affect retrieval effectiveness?
- **RQ2:** How effective is UrbanCross in terms of cross-domain adaptation? How does each component (e.g., source sampler, curriculum learning adjustment, adversarial training) contribute to UrbanCross’s domain adaptation capability?
- **RQ3:** How does each key hyperparameter (e.g., segmentation number, batch size, learning rate) affect UrbanCross?
- **RQ4:** How does UrbanCross’s domain adaptation capability affect satellite image-text retrieval qualitatively?

### 4.1 Experimental Setup

**4.1.1 Datasets.** To assess the efficacy of UrbanCross in satellite image-text retrieval, experiments were performed utilizing the RSICD [27] and RSITMD [47] datasets, which comprise 10,921 and 4,743 images, respectively. Our domain adaptation studies utilized the Skyscript benchmark dataset [43], which features 5.2 million

image-text pairs globally. To improve UrbanCross’s adaptability across diverse urban environments, we selected high-resolution images from Spain, Germany, and Finland (GSD  $\leq 0.5$  m/pixel), resulting in the creation of UC-Spain, UC-Finland, and UC-Germany datasets. These datasets contain 46,041 pairs of 1,621 types of geo-tags from various Spanish regions (ranging from the capital to smaller towns), 165,128 pairs of 3,033 types of geo-tags from Berlin, Germany, and 58,783 pairs of 5,826 types of geo-tags covering Finland, demonstrating a commitment to geographic diversity and data quality. Figure 4 displays data statistics and visualizations.

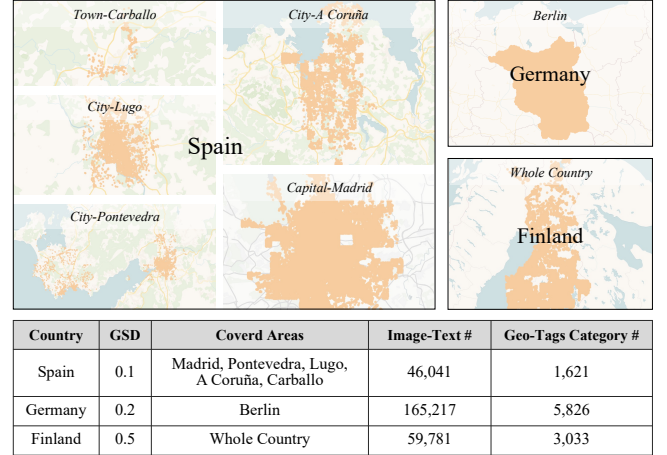


Figure 4: UrbanCross dataset statistics.

**4.1.2 Baselines.** We compare UrbanCross with the following baselines in satellite image-text retrieval:

- **LW-MCR** [48]: A lightweight algorithm is optimized for multi-scale information retrieval, leveraging insights from latent knowledge within various layers to enhance performance.
- **AMFMN** [46]: It utilizes a multiscale structure and a semantic alignment mechanism to filter out redundant information and align high-level image features with textual data.
- **GaLR** [49]: It incorporates global and local information through a multi-level dynamic fusion module, integrating features across different levels, ensuring a more comprehensive representation.
- **SWAN** [30]: It enhances scene perception and minimizes semantic confusion by introducing a scene-aware aggregation network with a new metric for scene-level retrieval performance.
- **PIR** [29]: It employs a Prior Instruction Representation framework with progressive attention encoders to improve feature representation and long-range dependency modeling, reducing semantic confusion with a cluster-wise attribution loss.
- **RemoteCLIP** [24]: The first vision-language foundational model designed specifically for satellite imagery, aiming for robust feature learning and accurate textual embedding alignment.

**4.1.3 Metrics and Implementation.** Essential metrics are employed to evaluate the performance of satellite image-text retrieval and the effectiveness of domain adaptation. The **R@K** metric, crucial for assessing the accuracy of satellite image-text retrieval, determines whether the correct answer is among the top K results. Mean Recall

**Table 1: Performance comparison of UrbanCross and the state-of-the-art methods on RSICD and RSITMD datasets using R@1, R@5, R@10, and Mean Recall metrics. Includes UrbanCross performance across datasets from Spain, Finland, and Germany, and effectiveness analysis of image segments from the Segment Anything Model via ablation experiments. Optimal and suboptimal performances are indicated by bold and underlined text, respectively.**

Testing Dataset	Training Dataset	Dataset Size #	Year	Method	Image Backbone	Text Backbone	Image to Text			Text to Image			Mean Recall
							R@1	R@5	R@10	R@1	R@5	R@10	
RSICD	RSICD	10,921	2021	LW-MCR	SqueezeNet	/	3.54	11.89	18.78	4.23	16.67	28.01	13.85
			2022	AMFMN	ResNet-18	GRU	5.33	13.92	20.23	4.01	16.12	28.32	14.66
			2022	GalR	ResNet-18	GRU	6.47	18.85	29.16	4.65	18.72	30.92	18.13
			2023	SWAN	ResNet-50	GRU	7.28	19.97	29.08	5.54	21.56	37.21	20.11
			2023	PIR	Swin-T + ResNet-50	BERT	9.97	27.32	39.33	7.01	24.53	38.88	24.51
			2024	UrbanCross-MMA w/o SEG	ViT-L-14	Transformer	17.52	<b>38.49</b>	<b>51.86</b>	<u>14.52</u>	<b>40.89</b>	<b>57.67</b>	<b>36.83</b>
	2024	UrbanCross-MMA	ViT-L-14	Transformer	<u>18.19 (-3.8%)</u>	<u>37.09 (-3.6%)</u>	<u>51.46 (-0.8%)</u>	14.14 (-2.6%)	39.85 (-2.6%)	56.43 (-2.2%)	36.19 (-1.7%)		
	2023	RET-3	165,745	RemoteCLIP	ResNet-50	Transformer	12.90	32.02	44.46	10.59	33.25	48.93	30.36
	2023	DET-10	RemoteCLIP	ViT-B-32	Transformer	17.14	<u>37.92</u>	<u>51.78</u>	13.77	37.10	54.15	35.31	
	2023	SEG-4	RemoteCLIP	ViT-L-14	Transformer	<b>18.42</b>	<b>37.48</b>	<b>51.12</b>	<b>14.69</b>	<b>40.03</b>	<b>56.62</b>	<b>36.39</b>	
RSITMD	RSITMD	4,743	2021	LW-MCR	SqueezeNet	/	10.11	25.58	39.87	7.52	30.23	50.78	27.35
			2022	AMFMN	ResNet-18	GRU	10.74	23.78	40.05	10.30	34.49	54.67	29.01
			2022	GalR	ResNet-18	GRU	11.76	29.28	41.45	9.68	35.88	54.03	30.35
			2023	SWAN	ResNet-50	GRU	13.29	30.69	45.90	10.12	39.30	60.43	33.29
			2023	PIR	Swin-T + ResNet-50	BERT	18.81	41.15	53.10	13.67	42.35	62.88	38.66
			2024	UrbanCross-MMA w/o SEG	ViT-L-14	Transformer	<b>27.98</b>	<b>51.68</b>	<b>65.56</b>	<u>23.66</u>	<u>58.44</u>	<u>73.78</u>	<b>50.18</b>
	2024	UrbanCross-MMA	ViT-L-14	Transformer	27.78 (-0.7%)	51.22 (-0.89%)	<b>66.44 (+1.43%)</b>	23.73 (+0.3%)	57.11 (-2.3%)	71.32 (-3.3%)	49.60 (-1.2%)		
	2023	RET-3	165,745	RemoteCLIP	ResNet-50	Transformer	22.79	47.79	61.95	19.42	51.64	70.58	45.70
	2023	DET-10	RemoteCLIP	ViT-B-32	Transformer	27.65	50.88	65.93	21.99	56.11	73.27	49.31	
	2023	SEG-4	RemoteCLIP	ViT-L-14	Transformer	27.88	51.55	63.27	23.63	<b>59.42</b>	<b>74.82</b>	50.10	
UC-Spain	Spain	46,041	2024	UrbanCross-MMA w/o SEG	ViT-L-14	Transformer	6.72	19.73	28.63	7.62	21.61	30.87	19.20
			2024	UrbanCross-MMA	ViT-L-14	Transformer	<b>7.81 (+16.2%)</b>	<b>22.12 (+12.1%)</b>	<b>31.98 (+11.7%)</b>	<b>8.44 (+10.8%)</b>	<b>23.79 (+10.1%)</b>	<b>33.6 (+8.8%)</b>	<b>21.29 (+10.9%)</b>
UC-Finland	Finland	59,781	2024	UrbanCross-MMA w/o SEG	ViT-L-14	Transformer	8.98	25.15	35.49	8.78	24.69	35.75	23.14
2024	UrbanCross-MMA	ViT-L-14	Transformer	<b>10.4 (+15.8%)</b>	<b>26.95 (+7.2%)</b>	<b>37.29 (+5.1%)</b>	<b>10.32 (+17.5%)</b>	<b>28.08 (+13.7%)</b>	<b>38.71 (+8.3%)</b>	<b>25.29 (+9.3%)</b>			
UC-Germany	Germany	165,217	2024	UrbanCross-MMA w/o SEG	ViT-L-14	Transformer	9.33	26.38	37.01	9.11	25.37	36.52	23.95
2024	UrbanCross-MMA	ViT-L-14	Transformer	<b>10.62 (+13.8%)</b>	<b>27.86 (+5.6%)</b>	<b>39.46 (+6.62%)</b>	<b>10.98 (+20.53%)</b>	<b>29.28 (+15.41%)</b>	<b>39.54 (+8.3%)</b>	<b>26.29 (+9.8%)</b>			

(MeanR), providing a comprehensive overview of performance, computes the average of R@1, R@5, and R@10 for both image-to-text and text-to-image satellite retrieval tasks.

Furthermore, to evaluate domain adaptation, UrbanCross is pre-trained on data from one country and tested in another, assessing the model’s capacity to generalize to different urban environments. Comparing MeanR performance—direct model transfer versus fine-tuning with a subset of target domain data—highlights significant enhancements in global urban analysis effectiveness.

Our framework is trained on NVIDIA A800 GPUs utilizing the Adam Optimizer, with hyperparameter adjustments based on each epoch’s performance on the validation set. During the multimodal pretraining stage, the initial learning rate is established at  $1e-6$ , implementing a dynamic reduction strategy with a weight decay of 0.3 every 10 epochs. Batch sizes are set at 40, spanning 15 epochs, with each image keeping segments num as 6. Threshold  $T_d$  and  $T_s$  are set to 0.2. In the domain adaptation fine-tuning phase, the learning rate is set at  $1e-7$ , spanning 5 epochs. The ratio, defined by the target batch size of 16 to the source batch size of 80, is 0.2.  $\beta$  of the loss function is set to 1. For the pretraining dataset, we split train:val:test=7:1:2, while for the fine-tuning dataset, we split train:val:test=2:1:7, to facilitate domain-adaptation fine-tuning under limited data scenarios.

## 4.2 RQ1: Retrieval Performance Evaluation

An empirical evaluation was performed to assess the performance of various models on satellite image-text retrieval tasks, utilizing the RSICD and RSITMD datasets. This evaluation aimed to benchmark

the effectiveness of the UrbanCross model against conventional methodologies. Additional experiments were conducted on the UC-Spain, UC-Finland, and UC-Germany datasets to establish benchmarks for future research. Importantly, this comparison excluded considerations of domain adaptation. The UrbanCross variant deployed in these assessments was UrbanCross-MMA (Multi-Modal Alignment), which excluded the domain adaptation stage. Furthermore, an ablation study was conducted to explore the impact of image segmentation on enhancing retrieval accuracy. The detailed results of these experiments are presented in Table 1.

- UrbanCross exhibits improved retrieval accuracy, surpassing the recent baseline, PIR, with mean recall improvements of 50.3% on RSICD dataset and 29.8% on RSITMD dataset, under equivalent training and testing conditions. Besides, it also demonstrates a modest enhancement over RemoteCLIP, which is trained on a larger dataset, highlighting its effective learning capabilities.
- The impact of SEG varies across datasets, depending on the quality of the data. For the RSICD and RSITMD datasets, adding segments for alignment decreases mean recall by 1.7% and 1.2%, respectively. This reduction is primarily attributed to the insufficient semantic information in the text, which hinders alignment with the fine-grained segment features, leading to broader contextual matching and, consequently, diminished returns.
- Conversely, the SEG-inclusive model excels in UC datasets with rich annotations, showing mean recall improvements of 10.9% in UC-Spain, 9.3% in UC-Finland, and 9.8% in UC-Germany. These gains highlight SEG’s importance in datasets requiring fine-grained visual-textual matching. Our method, characterized by

**Table 2: UrbanCross Domain Adaptation and Ablation Study: Assesses Mean Recall effects when omitting Source Sampler (SS), Curriculum Learning Adjustment (CL), and Adversarial Training (AT) in cross-domain retrieval. Underlined text denotes no domain adaptation; bold text denotes full domain adaptation.**

Domain Adaptation		Method	Image to Text			Text to Image			Mean
Source	Target		R@1	R@5	R@10	R@1	R@5	R@10	Recall
Finland 59,781 #	Spain 46,041 #	<u>UrbanCross-MMA</u>	<u>0.60</u>	<u>2.48</u>	<u>3.87</u>	<u>0.71</u>	<u>2.67</u>	<u>4.28</u>	<u>2.44</u>
		UrbanCross (w/o SS)	0.64 (+6.7%)	2.55 (+2.8%)	3.99 (+3.1%)	0.74 (+4.2%)	2.80 (+4.9%)	4.50 (+5.1%)	2.54 (+4.2%)
		UrbanCross (w/o CL)	0.66 (+10%)	2.62 (+5.6%)	4.08 (+5.4%)	0.76 (+7.0%)	2.88 (+7.9%)	4.64 (+8.4%)	2.61 (+7.0%)
		UrbanCross (w/o AT)	0.68 (+13.3%)	2.69 (+8.5%)	4.17 (+7.8%)	0.78 (+9.9%)	2.95 (+10.5%)	4.78 (+11.7%)	2.68 (+9.9%)
		<b>UrbanCross</b>	<b>0.71 (+18.3%)</b>	<b>2.82 (+13.7%)</b>	<b>4.35 (+13.7%)</b>	<b>0.82 (+15.5%)</b>	<b>3.08 (+15.4%)</b>	<b>5.02 (+17.3%)</b>	<b>2.80 (+15.0%)</b>
Germany 165,217 #	Spain 46,041 #	<u>UrbanCross-MMA</u>	<u>1.50</u>	<u>5.30</u>	<u>8.40</u>	<u>1.90</u>	<u>5.60</u>	<u>8.80</u>	<u>5.25</u>
		UrbanCross (w/o SS)	1.55 (+3.3%)	5.45 (+2.8%)	8.65 (+3.0%)	1.96 (+3.2%)	5.78 (+3.2%)	9.06 (+3.0%)	5.41 (+3.0%)
		UrbanCross (w/o CL)	1.60 (+6.7%)	5.60 (+5.7%)	8.90 (+6.0%)	2.02 (+6.3%)	5.96 (+6.4%)	9.32 (+6.1%)	5.73 (+9.1%)
		UrbanCross (w/o AT)	1.65 (+10.0%)	5.75 (+8.5%)	9.15 (+8.9%)	2.08 (+9.5%)	6.14 (+9.6%)	9.58 (+8.9%)	5.89 (+12.4%)
		<b>UrbanCross</b>	<b>1.72 (+14.7%)</b>	<b>6.10 (+15.1%)</b>	<b>9.66 (+15.0%)</b>	<b>2.19 (+15.3%)</b>	<b>6.46 (+15.4%)</b>	<b>10.16 (+15.5%)</b>	<b>6.05 (+15.2%)</b>
Germany 165,217 #	Finland 59,781 #	<u>UrbanCross-MMA</u>	<u>1.10</u>	<u>3.80</u>	<u>6.30</u>	<u>1.50</u>	<u>4.70</u>	<u>7.80</u>	<u>4.20</u>
		UrbanCross (w/o SS)	1.14 (+3.6%)	3.93 (+3.4%)	6.52 (+3.5%)	1.55 (+3.3%)	4.86 (+3.4%)	8.07 (+3.5%)	4.34 (+3.3%)
		UrbanCross (w/o CL)	1.18 (+7.3%)	4.06 (+6.8%)	6.74 (+7.0%)	1.60 (+6.7%)	5.02 (+6.8%)	8.34 (+6.9%)	4.49 (+6.9%)
		UrbanCross (w/o AT)	1.22 (+10.9%)	4.19 (+10.3%)	6.96 (+10.5%)	1.65 (+10.0%)	5.18 (+10.2%)	8.61 (+10.4%)	4.63 (+10.2%)
		<b>UrbanCross</b>	<b>1.27 (+15.5%)</b>	<b>4.39 (+15.5%)</b>	<b>7.28 (+15.6%)</b>	<b>1.73 (+15.3%)</b>	<b>5.42 (+15.3%)</b>	<b>9.00 (+15.4%)</b>	<b>4.85 (+15.5%)</b>

high-quality texts, geo-tags, and LMM integration, effectively enhances image-text alignment, especially in datasets with thorough semantics and contextual information, as shown by the improved recall figures for UrbanCross with SEG, demonstrating how image segmentation significantly improves the precision and relevance of data retrieval in environments with detailed visual and textual data.

### 4.3 RQ2: Cross-Domain Adaptability Evaluation

In this study section, we conducted experiments to evaluate the domain adaptation effectiveness of UrbanCross across various countries. The analysis leverages three main transfer scenarios: Finland to Spain, Germany to Spain, and Germany to Finland. Each scenario involves comparative ablation studies to understand the impact of each adaptation component: the Source Sampler (SS), Curriculum Learning Adjustment (CL), and Adversarial Training (AT). Detailed comparison data is shown in table 2. These findings demonstrate:

- **Overall Transferability Improvement:** UrbanCross demonstrates significant adaptability improvements in all scenarios when fully configured with SS, CL, and AT. For instance, complete configurations yield increases in mean recall of 15.0% for Finland to Spain, 15.2% for Germany to Spain, and 15.5% for Germany to Finland. These improvements underscore the model’s robustness in effectively managing domain shifts and enhancing retrieval accuracy across varied urban datasets.
- **Effectiveness of Source Sampler (SS):** The ablation of SS demonstrates the most significant decrease in performance enhancement compared to removing other components, emphasizing its critical role. As we can see, the presence of SS ensures that the model adapts to changes in data distribution from the source domain to the target domain. Without such adaptation,

the data gap between the source and target domains would lead to a decline in performance. Specifically, gains after removing SS are +4.2% for Finland to Spain, +3.0% for Germany to Spain, and +3.3% for Germany to Finland. These modest gains confirm the effectiveness of SS in bridging the data distribution gap between source and target domains.

- **Effectiveness of Curriculum Learning Adjustment (CL):** Removing CL results in higher performance gains than removing AT but lower than removing SS, placing it in the middle of the adaptation hierarchy. Specifically, the performance gains after removing CL are +7.0% for Finland to Spain, +9.1% for Germany to Spain, and +6.9% for Germany to Finland. This indicates that curriculum learning strategy allows the source sampler to dynamically adjust filter threshold, thus enhancing the learning difficulty. This guides the model to focus on more challenging examples in the later stages of training, thereby significantly improving domain adaptation performance.
- **Effectiveness of Adversarial Training (AT):** The exclusion of AT, while still maintaining SS and CL, shows the least impact on performance compared to the other components. The gains are +9.9% for Finland to Spain, +12.4% for Germany to Spain, and +10.2% for Germany to Finland. Although AT contributes to model robustness and generalization, its impact on performance enhancement is less significant than SS and CL, making it the least influential component in the adaptation process.

### 4.4 RQ3: Hyperparameter Study

The optimization process of UrbanCross’s hyperparameters is meticulously designed to enhance the mean recall, a critical performance metric. This process is comprehensively visualized in Figure 5, which delineates the adjustments and their impacts during both the pre-training and fine-tuning stages.

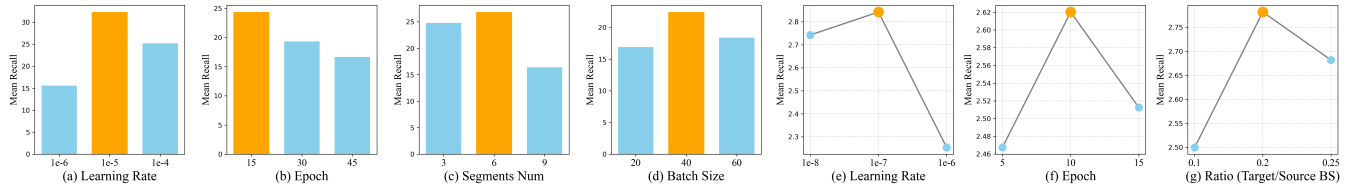


Figure 5: Impact of hyperparameters on Mean Recall during UrbanCross Pre-training (a-d) and Fine-tuning (e-g).

- Pre-training Stage:** Initial analysis examines the learning rate’s influence on model performance. A learning rate of 1e-5 optimizes mean recall, offering a balance between convergence speed and stability. Increasing the learning rate to 1e-4 results in diminished recall, indicative of surpassing optimal parameters. Additionally, extending pre-training beyond 30 epochs does not improve recall, signaling a dataset learning saturation point. The number of segments significantly influences performance; six segments are optimal for capturing pertinent patterns without overfitting. A batch size of 40 is ideal, striking a balance between computational efficiency and generalization capacity.
- Fine-tuning Stage:** The fine-tuning stage begins by examining the learning rate’s impact on model performance during domain adaptation. An optimal rate of 1e-7 refines parameters with minimal deviation. Extending fine-tuning beyond 10 epochs leads to overfitting, highlighted by decreased recall, emphasizing the need for moderation in epoch selection. A target-to-source batch size ratio of 0.2 (80/16) optimizes mean recall, balancing domain-specific learning with knowledge retention.

Through systematic experimentation during both the pre-training and fine-tuning stages, we identified optimal settings that maximize mean recall while ensuring model stability.

#### 4.5 RQ4: Qualitative Analysis

To demonstrate our method’s cross-domain efficacy, we provide two illustrative examples representing distinct settings: Finland to Spain and Germany to Finland, as depicted in Figure 6.

For the image query of an industrial roof with solar panels, using the pre-trained model from Finland directly in Spain, without domain adaptation, resulted in inferior outcomes and failed to accurately capture the solar panel concept. This discrepancy can be attributed to the climatic differences between Finland and Spain. Finland experiences limited annual sunlight and extended periods of darkness, particularly in winter, while Spain enjoys abundant sunshine and widespread solar energy adoption, resulting in frequent solar panel depictions in image-text pairs. By fine-tuning the model through domain adaptation with a small dataset from Spain, we achieved accurate textual descriptions. An analysis of the top four results reveals a consensus regarding the solar panel concept.

In the second example, assessing the model’s ability to interpret test query images underscores features characteristic of Finland, such as extensive snow cover and a vibrant winter sports scene featuring skiing, ice hockey, and ice skating. Conversely, the absence of comparable samples in Germany results in pre-fine-tuning images that emphasize superficial attributes like snow and whiteness, potentially yielding irrelevant results unrelated to ice sports. These

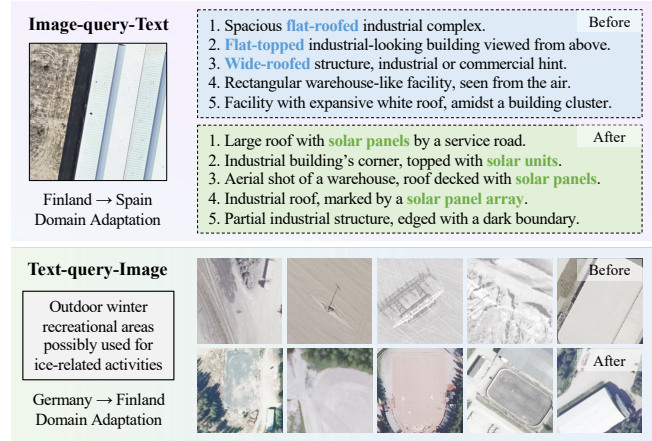


Figure 6: UrbanCross domain adaptation: before and after comparison. Top 5 retrieval results for image-to-text retrieval from Finland to Spain (above) and text-to-image retrieval from Germany to Finland (below).

images might portray snow-covered locations with no specific association with ice sports activities. Through fine-tuning, the model significantly enhances its precision in associating search text with locations related to ice sports.

## 5 CONCLUSION AND FUTURE WORK

This paper introduced UrbanCross, a novel framework designed for cross-domain satellite image-text retrieval, achieving enhancements at both data and model levels. At the data level, it integrates geo-tags and an LMM to enrich textual semantics and diversity, and employs SAM to maintain highly relevant visual features, thus ensuring improved alignment with text. At the model level, it incorporates fine-grained feature fusion for enhanced modal alignment and introduces a novel domain adaptation module that combines a Curriculum-based Source Sampler with Weighted Adversarial Cross-Domain Fine-tuning to effectively address the domain gap across various countries. Experimental results demonstrate that UrbanCross surpasses baseline models in retrieval performance and exhibits remarkable adaptability to diverse urban landscapes.

We aspire that this work will inspire future research in cross-domain satellite image-text retrieval frameworks on the following aspects: 1) Designing more precise curriculum learning strategy; 2) Exploring zero-shot cross-domain satellite image-text retrieval; 3) Empowering knowledge update via external knowledge base.



## REFERENCES

- [1] Mohsen Ahmadi, Ahmad Gholizadeh Lonbar, Abbas Sharifi, Ali Tarlani Beris, Mohammadsadeh Nouri, and Amir Sharifzadeh Javidi. 2023. Application of segment anything model for civil infrastructure defect assessment. *arXiv preprint arXiv:2304.12600* (2023).
- [2] Mohamad M Al Rahhal, Yakoub Bazi, Norah A Alsharif, Laila Bashmal, Naif Alajlan, and Farid Melgani. 2022. Multilanguage transformer for improved text to remote sensing image retrieval. *IEEE Journal of Selected Topics in Applied Earth Observations and Remote Sensing* 15 (2022), 9115–9126.
- [3] Min Cao, Shiping Li, Juntao Li, Liqiang Nie, and Min Zhang. 2022. Image-text retrieval: A survey on recent research and development. *arXiv preprint arXiv:2203.14713* (2022).
- [4] Jun Chen, Deyao Zhu, Xiaoqian Shen, Xiang Li, Zechun Liu, Pengchuan Zhang, Raghuraman Krishnamoorthi, Vikas Chandra, Yunyang Xiong, and Mohamed Elhoseiny. 2023. Minigpt-v2: large language model as a unified interface for vision-language multi-task learning. *arXiv preprint arXiv:2310.09478* (2023).
- [5] Keyan Chen, Chenyang Liu, Hao Chen, Haotian Zhang, Wenyuan Li, Zhengxia Zou, and Zhenwei Shi. 2024. RSPrompter: Learning to prompt for remote sensing instance segmentation based on visual foundation model. *IEEE Transactions on Geoscience and Remote Sensing* (2024).
- [6] Keqin Chen, Zhao Zhang, Weili Zeng, Richong Zhang, Feng Zhu, and Rui Zhao. 2023. Shikra: Unleashing Multimodal LLM's Referential Dialogue Magic. *arXiv preprint arXiv:2306.15195* (2023).
- [7] Lin Chen, Jisong Li, Xiaoyi Dong, Pan Zhang, Conghui He, Jiaqi Wang, Feng Zhao, and Dahua Lin. 2023. ShareGPT4V: Improving Large Multi-Modal Models with Better Captions. *arXiv preprint arXiv:2311.12793* (2023).
- [8] Yaxiong Chen, Jinghao Huang, Xiaoyu Li, Shengwu Xiong, and Xiaoqiang Lu. 2023. Multiscale Salient Alignment Learning for Remote Sensing Image-Text Retrieval. *IEEE Transactions on Geoscience and Remote Sensing* (2023).
- [9] Qimin Cheng, Yuzhuo Zhou, Peng Fu, Yuan Xu, and Liang Zhang. 2021. A deep semantic alignment network for the cross-modal image-text retrieval in remote sensing. *IEEE Journal of Selected Topics in Applied Earth Observations and Remote Sensing* 14 (2021), 4284–4297.
- [10] Wenliang Dai, Junnan Li, Dongxu Li, Anthony Meng Huat Tiong, Junqi Zhao, Weisheng Wang, Boyang Li, Pascale Fung, and Steven Hoi. 2023. InstructBLIP: Towards General-purpose Vision-Language Models with Instruction Tuning. *arXiv:2305.06500* [cs.CV]
- [11] Guhao Feng, Bohang Zhang, Yuntian Gu, Haotian Ye, Di He, and Liwei Wang. 2024. Towards revealing the mystery behind chain of thought: a theoretical perspective. *Advances in Neural Information Processing Systems* 36 (2024).
- [12] Peng Gao, Jiaming Han, Renrui Zhang, Ziyi Lin, Shijie Geng, Aojun Zhou, Wei Zhang, Pan Lu, Conghui He, Xiangyu Yue, et al. 2023. Llama-adapter v2: Parameter-efficient visual instruction model. *arXiv preprint arXiv:2304.15010* (2023).
- [13] Xixuan Hao, Wei Chen, Yibo Yan, Siru Zhong, Kun Wang, Qingsong Wen, and Yuxuan Liang. 2024. UrbanVLP: A Multi-Granularity Vision-Language Pre-Trained Foundation Model for Urban Indicator Prediction. *arXiv preprint arXiv:2403.16831* (2024).
- [14] Liu He, Shuyuan Liu, Ran An, Yudong Zhuo, and Jian Tao. 2023. An End-to-End Framework Based on Vision-Language Fusion for Remote Sensing Cross-Modal Text-Image Retrieval. *Mathematics* 11, 10 (2023), 2279.
- [15] Jack Hessel, Ari Holtzman, Maxwell Forbes, Roman Le Bras, and Yejin Choi. 2021. CLIPScore: A Reference-free Evaluation Metric for Image Captioning. In *Proceedings of the 2021 Conference on Empirical Methods in Natural Language Processing*, Marie-Francine Moens, Xuanjing Huang, Lucia Specia, and Scott Wen-tau Yih (Eds.). Association for Computational Linguistics, Online and Punta Cana, Dominican Republic, 7514–7528. <https://doi.org/10.18653/v1/2021.emnlp-main.595>
- [16] Yuan Hu, Jianlong Yuan, Congcong Wen, Xiaonan Lu, and Xiang Li. 2023. Rsgpt: A remote sensing vision language model and benchmark. *arXiv preprint arXiv:2307.15266* (2023).
- [17] Xinyu Huang, Youcai Zhang, Jinyu Ma, Weiwei Tian, Rui Feng, Yuejie Zhang, Yaqian Li, Yandong Guo, and Lei Zhang. 2024. Tag2Text: Guiding Vision-Language Model via Image Tagging. In *The Twelfth International Conference on Learning Representations*. <https://openreview.net/forum?id=x6u2BQ7xcq>
- [18] Robin Jarry, Marc Chaumont, Laure Berti-Équille, and Gérard Subsol. 2021. Assessment of CNN-based methods for poverty estimation from satellite images. In *International Conference on Pattern Recognition*. Springer, 550–565.
- [19] Neal Jean, Marshall Burke, Michael Xie, W Matthew Davis, David B Lobell, and Stefano Ermon. 2016. Combining satellite imagery and machine learning to predict poverty. *Science* 353, 6301 (2016), 790–794.
- [20] Wei Ji, Yinwei Wei, Zhedong Zheng, Hao Fei, and Tat-seng Chua. 2023. Deep multimodal learning for information retrieval. In *Proceedings of the 31st ACM International Conference on Multimedia*. 9739–9741.
- [21] Alexander Kirillov, Eric Mintun, Nikhila Ravi, Hanzi Mao, Chloe Rolland, Laura Gustafson, Tete Xiao, Spencer Whitehead, Alexander C. Berg, Wan-Yen Lo, Piotr Dollár, and Ross Girshick. 2023. Segment Anything. *arXiv:2304.02643* [cs.CV]
- [22] Yongqi Li, Wenjie Wang, Leigang Qu, Liqiang Nie, Wenjie Li, and Tat-Seng Chua. 2024. Generative Cross-Modal Retrieval: Memorizing Images in Multimodal Language Models for Retrieval and Beyond. *arXiv preprint arXiv:2402.10805* (2024).
- [23] Yunpeng Li, Xiangrong Zhang, Jing Gu, Chen Li, Xin Wang, Xu Tang, and Licheng Jiao. 2021. Recurrent attention and semantic gate for remote sensing image captioning. *IEEE Transactions on Geoscience and Remote Sensing* 60 (2021), 1–16.
- [24] Fan Liu, Delong Chen, Zhangqingyun Guan, Xiaocong Zhou, Jiale Zhu, and Jun Zhou. 2023. RemoteCLIP: A Vision Language Foundation Model for Remote Sensing. *arXiv preprint arXiv:2306.11029* (2023).
- [25] Haotian Liu, Chunyuan Li, Yuheng Li, and Yong Jae Lee. 2023. Improved baselines with visual instruction tuning. *arXiv preprint arXiv:2310.03744* (2023).
- [26] Haotian Liu, Chunyuan Li, Qingyang Wu, and Yong Jae Lee. 2023. Visual instruction tuning. *arXiv preprint arXiv:2304.08485* (2023).
- [27] Xiaoqiang Lu, Binqiang Wang, Xiangtao Zheng, and Xuelong Li. 2018. Exploring Models and Data for Remote Sensing Image Caption Generation. *IEEE Transactions on Geoscience and Remote Sensing* 56, 4 (April 2018), 2183–2195. <https://doi.org/10.1109/tgrs.2017.2776321>
- [28] Li Mi, Siran Li, Christel Chappuis, and Devis Tuia. 2022. Knowledge-Aware Cross-Modal Text-Image Retrieval for Remote Sensing Images. In *Proceedings of the Second Workshop on Complex Data Challenges in Earth Observation (CDCEO 2022)*.
- [29] Jiancheng Pan, Qing Ma, and Cong Bai. 2023. A Prior Instruction Representation Framework for Remote Sensing Image-text Retrieval. In *Proceedings of the 31st ACM International Conference on Multimedia*. 611–620.
- [30] Jiancheng Pan, Qing Ma, and Cong Bai. 2023. Reducing semantic confusion: Scene-aware aggregation network for remote sensing cross-modal retrieval. In *Proceedings of the 2023 ACM International Conference on Multimedia Retrieval*. 398–406.
- [31] Sinno Jialin Pan and Qiang Yang. 2009. A survey on transfer learning. *IEEE Transactions on knowledge and data engineering* 22, 10 (2009), 1345–1359.
- [32] Zhiliang Peng, Wenhui Wang, Li Dong, Yaru Hao, Shaohan Huang, Shuming Ma, and Furu Wei. 2023. Kosmos-2: Grounding Multimodal Large Language Models to the World. *arXiv preprint arXiv:2306.14824* (2023).
- [33] Alec Radford, Jong Wook Kim, Chris Hallacy, Aditya Ramesh, Gabriel Goh, Sandhini Agarwal, Girish Sastry, Amanda Askell, Pamela Mishkin, Jack Clark, et al. 2021. Learning transferable visual models from natural language supervision. In *International conference on machine learning*. PMLR, 8748–8763.
- [34] Felix Rembold, Clement Atzberger, Igor Savin, and Oscar Rojas. 2013. Using low resolution satellite imagery for yield prediction and yield anomaly detection. *Remote Sensing* 5, 4 (2013), 1704–1733.
- [35] Mark Sabini, Gili Ruskak, and Brad Ross. 2017. Understanding satellite-imagery-based crop yield predictions. *Stanford* (2017).
- [36] João Daniel Silva, João Magalhães, Devis Tuia, and Bruno Martins. 2024. Large Language Models for Captioning and Retrieving Remote Sensing Images. *arXiv preprint arXiv:2402.06475* (2024).
- [37] Yihong Tang, Ao Qu, Andy HF Chow, William HK Lam, Sze Chun Wong, and Wei Ma. 2022. Domain adversarial spatial-temporal network: A transferable framework for short-term traffic forecasting across cities. In *Proceedings of the 31st ACM International Conference on Information & Knowledge Management*. 1905–1915.
- [38] Ashish Vaswani, Noam Shazeer, Niki Parmar, Jakob Uszkoreit, Llion Jones, Aidan N Gomez, Lukasz Kaiser, and Illia Polosukhin. 2017. Attention is all you need. *Advances in neural information processing systems* 30 (2017).
- [39] Di Wang, Qiming Zhang, Yufei Xu, Jing Zhang, Bo Du, Dacheng Tao, and Liangpei Zhang. 2022. Advancing plain vision transformer toward remote sensing foundation model. *IEEE Transactions on Geoscience and Remote Sensing* 61 (2022), 1–15.
- [40] Leye Wang, Xu Geng, Xiaojuan Ma, Feng Liu, and Qiang Yang. 2018. Cross-city transfer learning for deep spatio-temporal prediction. *arXiv preprint arXiv:1802.00386* (2018).
- [41] Leye Wang, Bin Guo, and Qiang Yang. 2018. Smart city development with urban transfer learning. *Computer* 51, 12 (2018), 32–41.
- [42] Qi Wang, Wei Huang, Xueting Zhang, and Xuelong Li. 2020. Word-sentence framework for remote sensing image captioning. *IEEE Transactions on Geoscience and Remote Sensing* 59, 12 (2020), 10532–10543.
- [43] Zhecheng Wang, Rajanie Prabha, Tianyuan Huang, Jiajun Wu, and Ram Rajagopal. 2023. Skyscript: A large and semantically diverse vision-language dataset for remote sensing. *arXiv preprint arXiv:2312.12856* (2023).
- [44] Yibo Yan, Haomin Wen, Siru Zhong, Wei Chen, Haodong Chen, Qingsong Wen, Roger Zimmermann, and Yuxuan Liang. 2023. When urban region profiling meets large language models. *arXiv preprint arXiv:2310.18340* (2023).
- [45] Qinghao Ye, Haiyang Xu, Guohai Xu, Jiabo Ye, Ming Yan, Yiyang Zhou, Junyang Wang, Anwen Hu, Pengcheng Shi, Yaya Shi, et al. 2023. mplug-owl: Modularization empowers large language models with multimodality. *arXiv preprint arXiv:2304.14178* (2023).
- [46] Zhiqiang Yuan, Wenkai Zhang, Kun Fu, Xuan Li, Chubo Deng, Hongqi Wang, and Xian Sun. 2022. Exploring a fine-grained multiscale method for cross-modal

- remote sensing image retrieval. *arXiv preprint arXiv:2204.09868* (2022).
- [47] Zhiqiang Yuan, Wenkai Zhang, Kun Fu, Xuan Li, Chubo Deng, Hongqi Wang, and Xian Sun. 2022. Exploring a Fine-Grained Multiscale Method for Cross-Modal Remote Sensing Image Retrieval. *IEEE Transactions on Geoscience and Remote Sensing* 60 (2022), 1–19. <https://doi.org/10.1109/tgrs.2021.3078451>
- [48] Zhiqiang Yuan, Wenkai Zhang, Xuee Rong, Xuan Li, Jialiang Chen, Hongqi Wang, Kun Fu, and Xian Sun. 2021. A lightweight multi-scale crossmodal text-image retrieval method in remote sensing. *IEEE Transactions on Geoscience and Remote Sensing* 60 (2021), 1–19.
- [49] Zhiqiang Yuan, Wenkai Zhang, Changyuan Tian, Xuee Rong, Zhengyuan Zhang, Hongqi Wang, Kun Fu, and Xian Sun. 2022. Remote sensing cross-modal text-image retrieval based on global and local information. *IEEE Transactions on Geoscience and Remote Sensing* 60 (2022), 1–16.
- [50] Yang Zhan, Zhitong Xiong, and Yuan Yuan. 2024. Skyegypt: Unifying remote sensing vision-language tasks via instruction tuning with large language model. *arXiv preprint arXiv:2401.09712* (2024).
- [51] Xin Zhang, Yu Liu, Yuming Lin, Qingming Liao, and Yong Li. 2024. UV-SAM: Adapting Segment Anything Model for Urban Village Identification. *arXiv preprint arXiv:2401.08083* (2024).
- [52] Weixun Zhou, Haiyan Guan, Ziyu Li, Zhenfeng Shao, and Mahmoud R Delavar. 2023. Remote Sensing Image Retrieval in the Past Decade: Achievements, Challenges, and Future Directions. *IEEE Journal of Selected Topics in Applied Earth Observations and Remote Sensing* (2023).
- [53] Xingchen Zou, Yibo Yan, Xixuan Hao, Yuehong Hu, Haomin Wen, Erdong Liu, Junbo Zhang, Yong Li, Tianrui Li, Yu Zheng, et al. 2024. Deep Learning for Cross-Domain Data Fusion in Urban Computing: Taxonomy, Advances, and Outlook. *arXiv preprint arXiv:2402.19348* (2024).

## A APPENDIX

### A.1 Text Generation Analysis

**A.1.1 LMM Selection Evaluation.** The effectiveness of Large Multimodal Models (LMMs) in generating textual descriptions from images is crucial for cross-modal retrieval. To identify the most effective LMM for our research, we conducted a comparative analysis of prominent open-source models. This evaluation centered on the *PerceptionScore*, an innovative metric that quantifies the perceptual alignment of text with corresponding visual elements [13].

The *PerceptionScore* combines CLIPScore [15], utilizing the robust zero-shot capabilities of CLIP [33] for text quality assessment, with CycleScore. CycleScore aims to capture the visual recall of text, providing a comprehensive representation of salient image details. This metric enables thorough evaluation of textual descriptions by focusing on the absence of specific image elements, enhancing the alignment between text and image content.

**Table 3: Perception score of representative LMMs.**

Models	Average Generated Caption Scores
LLaVA-v1.5 [25]	0.674
mPLUG-Owl [45]	0.662
LLaMA-Adapter V2 [12]	0.698
MiniGPTv2 [4]	0.693
ShareGPT4V [7]	0.714
<b>InstructBLIP [10]</b>	<b>0.758</b>

Our experimental result, outlined in Table 3, indicates that InstructBLIP [10] surpasses other models with the highest *PerceptionScore*. Consequently, we adopted InstructBLIP as our Image-to-Text model, due to its superior ability to generate perceptually coherent and contextually rich descriptions, a fundamental attribute for advancing image-text alignment in our UrbanCross framework.

**A.1.2 Prompt Design Comparison.** As shown in Figure 7, we conduct a comparison of various prompt designs aimed at providing a comprehensive overview of a specific location depicted in satellite imagery. We present two straightforward methods for prompt design: one involves prompting the LMM to generate its visual interpretation, while the other directs its attention toward geological features. However, both of these initial prompts lack the capacity to elicit nuanced information from the LMM. To address this limitation, we incorporate geo-tags information into our prompt, tailoring it to each individual satellite image. As a result, the location description becomes sufficiently detailed to discern diverse semantic nuances within the image itself.

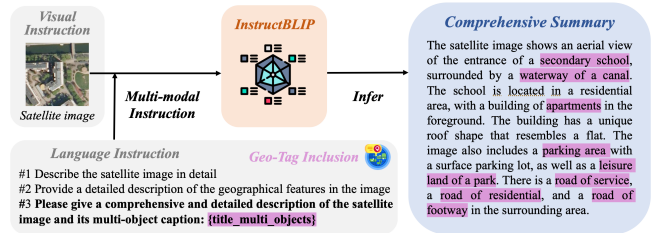


**Figure 7: Prompt cases for location description generation.**

**A.1.3 LMM Limitation Analysis.** As illustrated in Figure 8, our comprehensive analysis identifies specific scenarios where the Large Multimodal Models (LMMs) may exhibit suboptimal performance in generating text. This detailed investigation is designed to deepen our understanding of the LMM’s capabilities as well as its limitations. Within this context, we have pinpointed three distinct scenarios that illustrate these challenges.

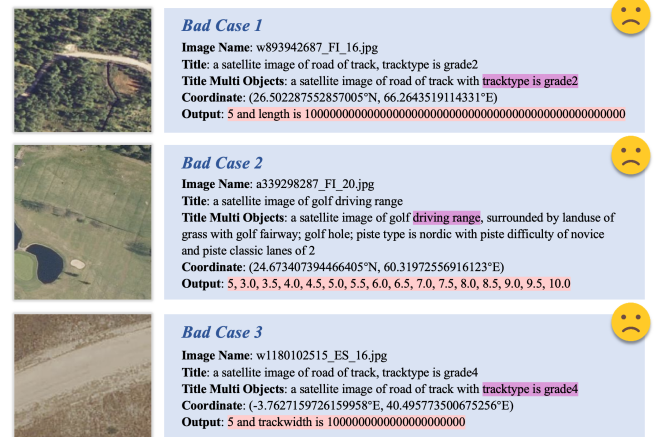


**Figure 8: Bad examples of geo-tags enhanced text description generated by InstructBLIP.**

- **Case 1.** When the Title Multi Objects contain elements outside the LMM’s pretraining data (e.g., "tracktype is grade2"), there is a risk of generating nonsensical descriptions.
- **Case 2:** When a term within the Title Multi Objects is polysemous (e.g., "driving range"), the LMM may misinterpret its meaning, resulting in incorrect text generation.

- **Case 3:** If the satellite image itself presents complexities that are difficult for human interpretation, particularly when accompanied by misleading geo-tags information, the resultant descriptions can be significantly degraded.

The causes of the aforementioned issues can be summarized as follows. Firstly, certain details in satellite images pose inherent challenges for human perception. Additionally, there is the issue of "hallucination" within the LMM itself, constrained by the capacity limitations of multimodal foundational models.

## A.2 Image Segmentation Analysis

**A.2.1 Image Segmentation and Text Enhancement.** The integration of image segmentation and geo-tags enrichment is essential for generating semantically rich text descriptions that align precisely with visual data. Figure 9 presents a set of illustrative examples demonstrating this intricate interplay. In the top image, we observe a school area, where segmentation and corresponding geo-tags annotations such as "natural: scrub", "building: school", and "leisure: park" provide a detailed textual narrative. This enriching process allows for the precise capture of the surrounding environment, highlighting not just the main amenity but also peripheral elements such as adjacent roads and recreational areas.

Similarly, the bottom image showcases a healthcare facility marked by geo-tags indicating a "healthcare: laboratory" and "leisure: pitch", offering valuable insights into the facility's functionality and layout. These geo-tags are instrumental in guiding the segmentation algorithm to prioritize and detail salient features within the scene, such as parking amenities and service roads, which are pivotal for a comprehensive understanding of the landscape.



**Figure 9: Illustrative examples of our image segments and geo-tags enhanced descriptions.**

By integrating geo-tags information, we not only refine the image segmentation but also enable the generation of text that captures a more granular and accurate depiction of the scene. This synergy between visual segmentation and textual enrichment is particularly evident when dealing with complex scenes where multiple objects or features must be precisely identified and described.

However, our methodology extends beyond simple annotation of images with geo-tags. It involves an iterative refinement where image segmentation informs the geo-tag-based text generation, and vice versa, leading to a fine-grained alignment that is greater

than the sum of its parts. Such alignment is crucial for applications requiring detailed and context-aware descriptions of geographical spaces, as it allows for a nuanced interpretation of the environment, which is critical for accurate satellite image-text retrieval tasks.

**A.2.2 Fine-tuning Segmentation Parameters.** Our methodical calibration of the image segmentation process has conclusively established that six segments ( $num\_seg = 6$ ) provide the optimal representation of scenes for our modeling purposes. This specific number of segments was meticulously selected to adeptly capture the inherent complexity of diverse landscapes while avoiding the overburdening of the model with extraneous, non-essential details. The solid rationale behind this particular parameter choice is vividly demonstrated and well-supported by the statistical distributions, which are thoroughly illustrated in Figure 10.

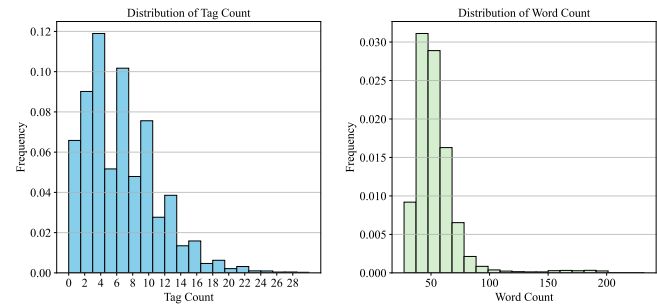


**Figure 10: Statistical distribution of tag count and word count of descriptions in our dataset, illustrating the optimal balance of information richness and brevity.**

The histogram on the left displays the frequency distribution of tag counts across our dataset. The majority of images have a tag count that clusters between four and ten, with a peak at six. This peak indicates that six tags often provide enough information to describe the essential elements of a scene without introducing noise through over-segmentation. The histogram on the right complements this finding by showing the word count distribution of the corresponding text descriptions. The majority of descriptions average approximately 54 words, achieving a balance between conciseness and detail necessary to comprehensively represent the scene for algorithmic processing and user interpretation.

This dual analysis of tag and word count distributions allows us to tailor our segmentation to align closely with the amount of detail that can be effectively described in texts, optimizing both the accuracy of image descriptions and the efficiency of our model. This fine-tuning ensures that each segment adds meaningful information to the generated description, facilitating a high level of detail in the semantic understanding of the scene, which is crucial for tasks such as image-text retrieval and scene comprehension.

**A.2.3 Future Segmentation Challenges.** While current segmentation approaches yield substantial improvements in text-image alignment, several challenges remain. These include poor segmentation performance for small objects, a lack of quantified metrics for assessing text quality, and the absence of an automatic refinement mechanism for the segmentation process. Addressing these issues will be crucial for future advancements. In subsequent iterations, tags could play a more pivotal role in guiding the joint training of image-text

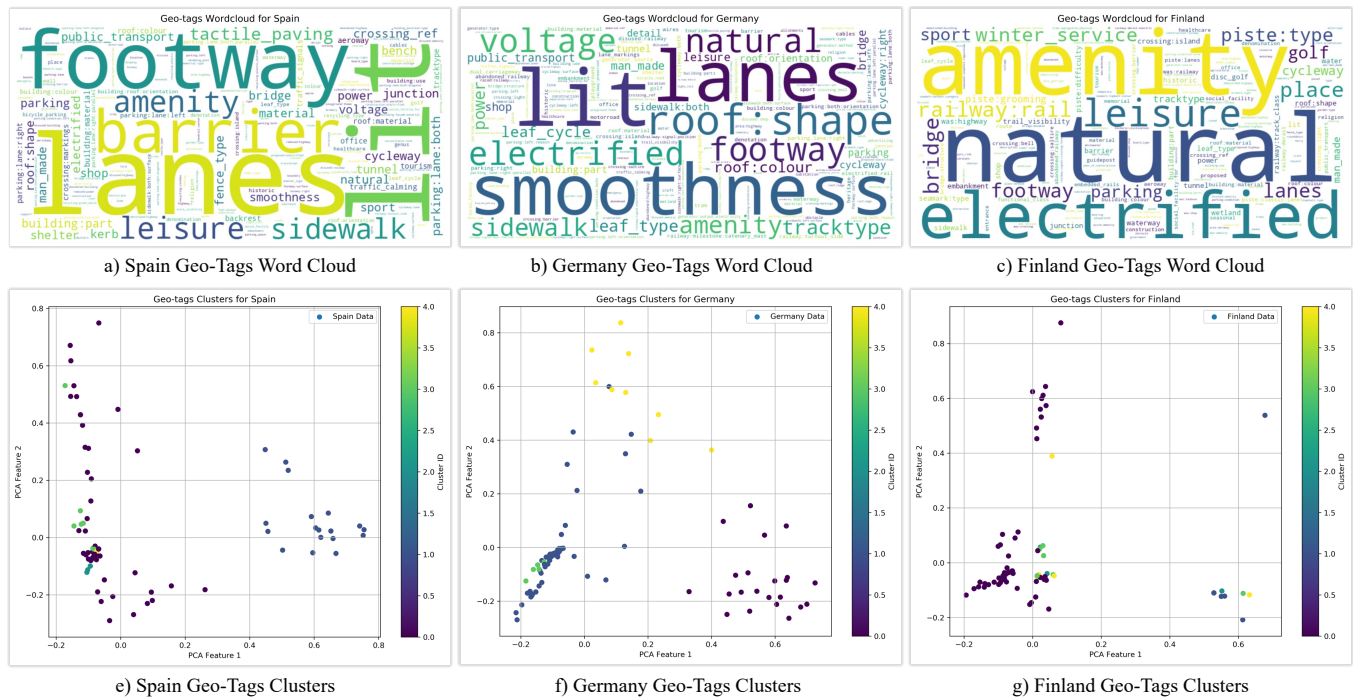


**Figure 11: Geo-Tags Word Cloud: Visualizing the Most Frequent Tags for Spain (a), Germany (b), and Finland (c); and Geo-Tags Clusters: Spatial Distribution Based on PCA for Spain (e), Germany (f), and Finland (g) across three countries.**

pairs [17]. Moreover, the adoption of a Chain-of-Thought mechanism [11], which leverages feedback based on segmentation ratios, could enhance text quality further. These strategies offer promising avenues for improving the functionality and efficiency of our segmentation techniques.

### A.3 Geo-Tags Analysis

**A.3.1 Geo-Tags Distribution and Cluster Insights.** In exploring geospatial metadata, geo-tags are pivotal in mining geospatial metadata to extract geographic semantics from satellite imagery. Our study applies frequency analysis to geo-tags from satellite images across three distinct European regions: Finland, Germany, and Spain. Using word clouds and PCA clustering, we effectively visualize the tag distribution and frequency, thereby highlighting the most prominent geographical features captured within the imagery.

Word clouds and PCA clustering diagrams provide dual modalities for in-depth visual analysis. Word clouds are particularly effective for quickly identifying the most frequent and prominent geo-tags, with larger font sizes indicating higher frequencies. This visualization technique is augmented by PCA clustering, which groups geo-tags based on the similarity of their occurrences across various images, revealing underlying patterns that may not be immediately evident from the word clouds alone.

For instance, word clouds for Finland, Germany, and Spain showcase a distinct predominance of tags such as "natural", "building", and "waterway", amongst others. However, the PCA clustering diagrams further elucidate the relationships between these tags. In the case of Finland, the PCA clustering diagram shows that geo-tags associated with "piste:type" and "winter\_service" cluster together

separately from common tags, highlighting the distinctive winter sports environment in the area.

The clustering technique used in this analysis involves a multi-step process. Initially, the frequency of geo-tags is computed from the dataset, and a high-dimensional vector space is created. This space is then simplified to two principal components through PCA, capturing the most significant variances among the geo-tags. Subsequently, the clustering algorithm subsequently divides these tags into coherent clusters, each marked by a unique color.

**A.3.2 Semantic Insights of Geo-Tags.** The insights from the word cloud and PCA clustering analyses significantly enhance our understanding of image-text alignment in cross-modal retrieval tasks. Specifically, PCA clustering illustrates the semantic proximity of geo-tags within their clusters, indicating potential shared functionalities or relationships. These insights not only emphasize the diverse geographical semantics inherent to the studied countries but also have profound implications for cross-modal retrieval tasks.

By leveraging clustering insights, searches for "recreational areas" could, for instance, pull images tagged with "leisure", "park", and "natural", knowing these tags share semantic relationships.

In summary, the comprehensive frequency and cluster analysis of geo-tags not only lay a foundational layer for semantic comprehension but also illustrates distinct geographical semantics across various countries. This is crucial for enhancing cross-modal retrieval tasks. Furthermore, the refined analytical methods employed in this study pave the way for extracting more nuanced and contextually rich insights from geo-tagged data, significantly enriching the narratives that can be derived from satellite imagery.